**Supporting Information**

# Influence of gold on the reactivity behavior of ceria nanorods in CO oxidation: Combining *operando* spectroscopies and DFT calculations

Marc Ziemba, Christian Hess*

Eduard-Zintl-Institute of Inorganic and Physical Chemistry, Technical University of Darmstadt, Alarich-Weiss-Str. 8, 64287 Darmstadt, Germany

*email: christian.hess@tu-darmstadt.de

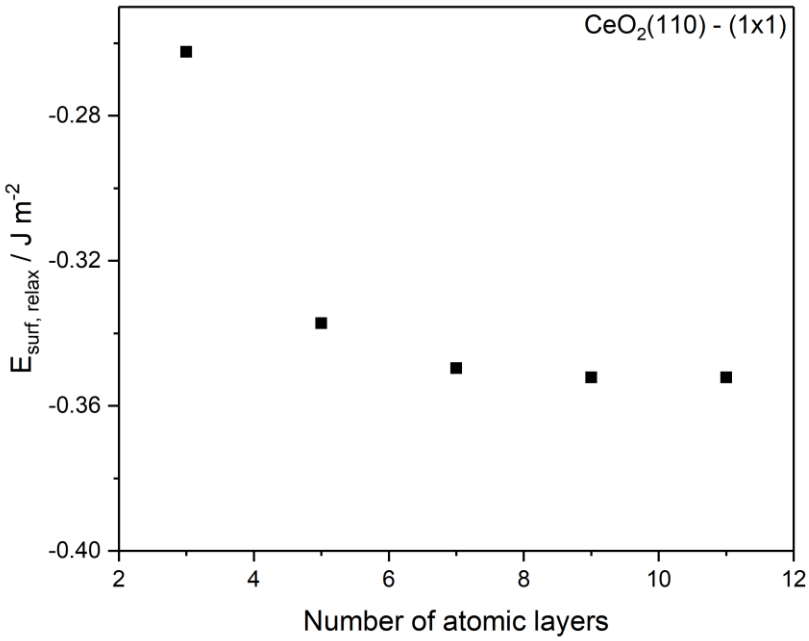


**Figure S1:** Representation of the relaxation energy $E_{surf, relax}$ of $CeO_2(110)$ structures with (1x1) periodicities as a function of the number of atomic layers.

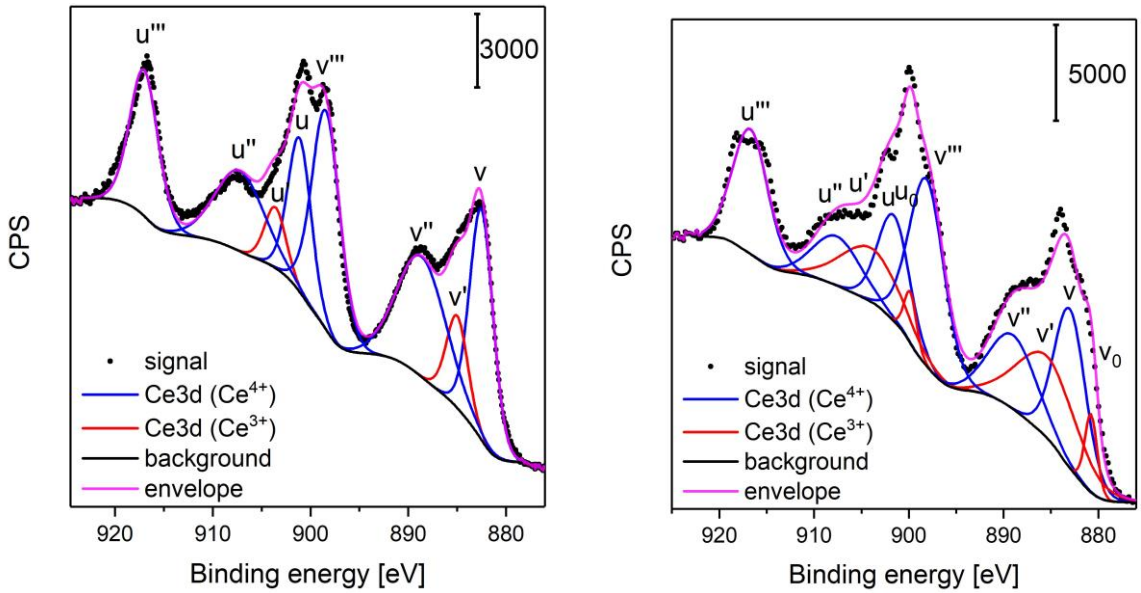


**Figure S2:** Ce3d photoemission of the bare ceria cubes (left) and the gold loaded cubes (right). Data is represented by black dots, and the background by a black line. A fitting analysis yields $Ce^{3+}$ (red) and $Ce^{4+}$ (blue) contributions as indicated. The envelope of all contributions in shown in magenta.

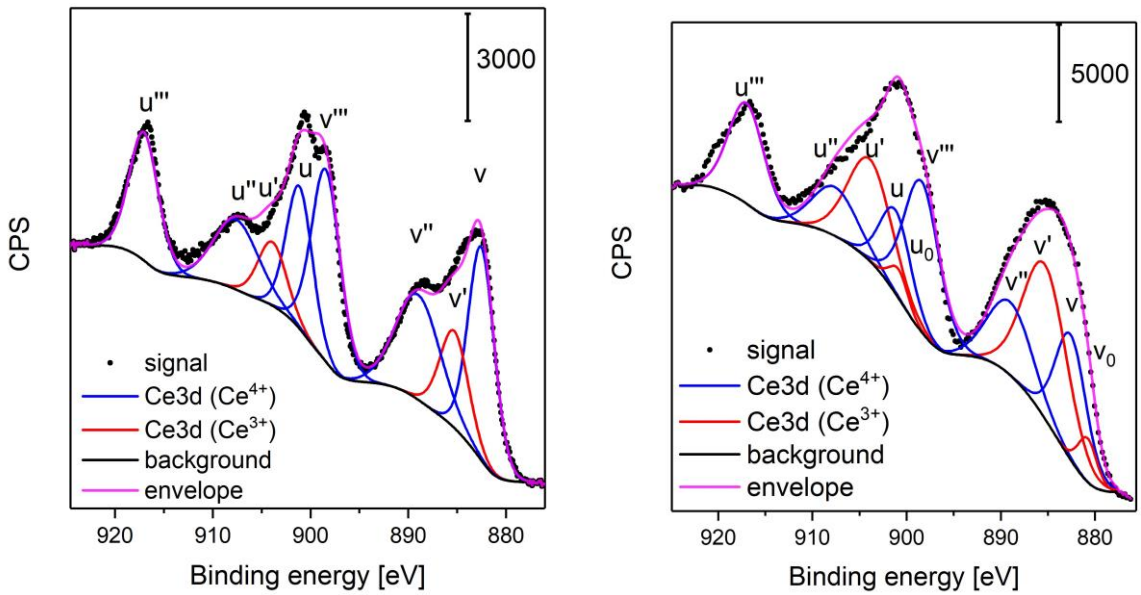


**Figure S3:** Ce3d photoemission of the bare ceria rods (left) and of the gold loaded rods (right). Data is represented by black dots, and the background by a black line. A fitting analysis yields $Ce^{3+}$ (red) and $Ce^{4+}$ (blue) contributions as indicated. The envelope of all contributions in shown in magenta.

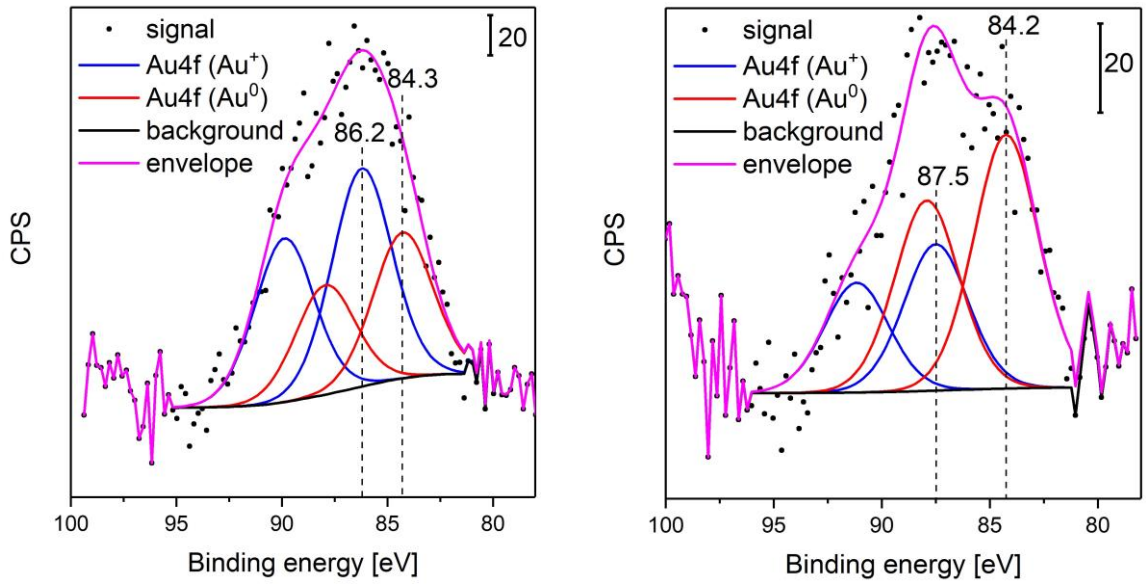


**Figure S4:** Au4f photoemission of the gold loaded cubes (left) and rods (right). Data is represented by black dots, and the background by a black line and the envelope of all contributions in shown in magenta. Blue curves correspond to the signal of cationic gold and red curves to the signal of metallic gold. The positions of the $Au4f_{7/2}$ signals are indicated.

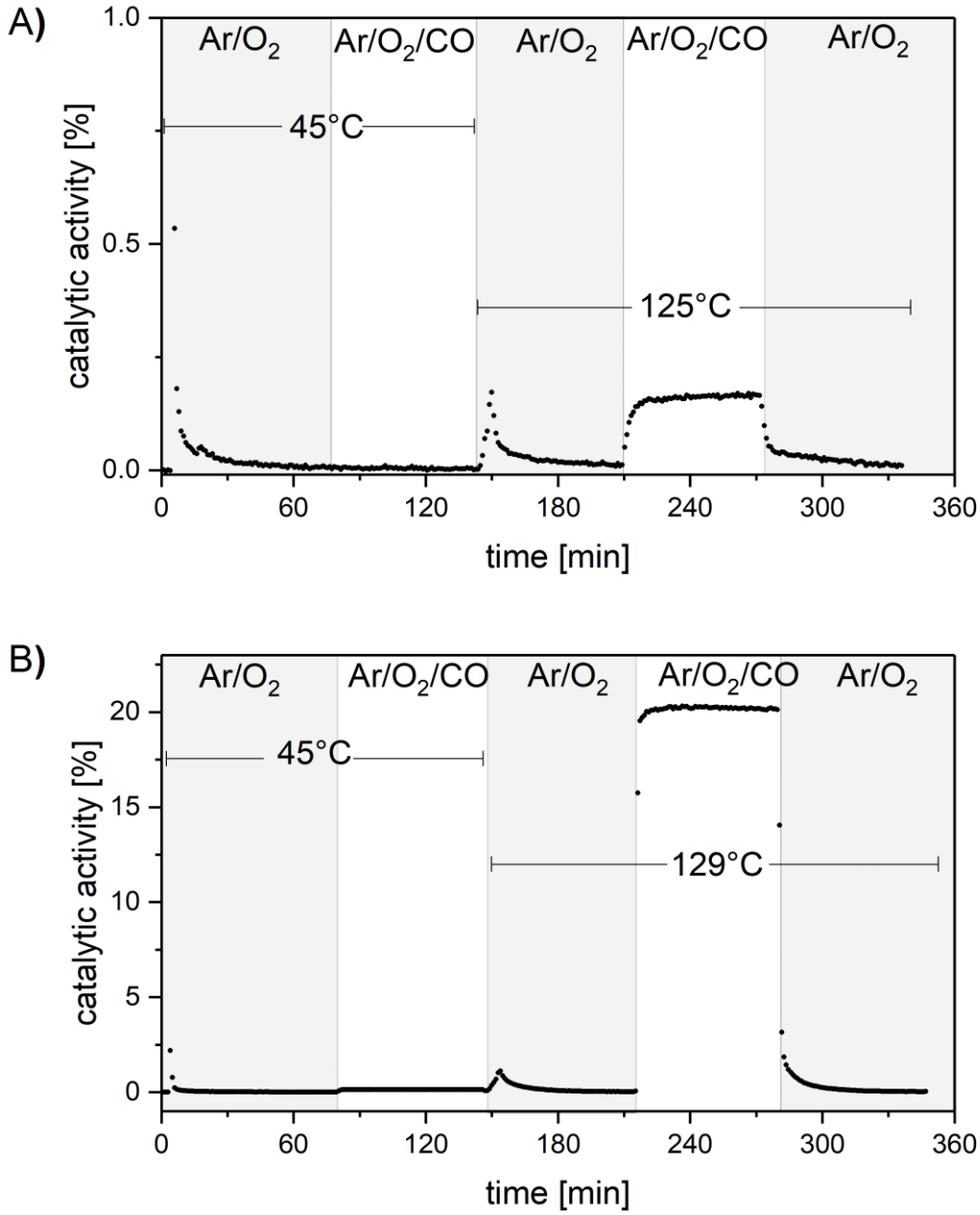


**Figure S5:** Catalytic activity during CO oxidation over **A)** $CeO_2$ nanocubes at 45 °C and 125 °C, and **B)** 0.3 wt% Au/$CeO_2$ nanocubes at 45 °C and 129 °C. The samples were exposed to a CO/$O_2$/Ar stream (2% CO, 25% $O_2$, Ar; 100 mL/min) under reaction conditions and to an $O_2$/Ar stream (25% $O_2$, Ar; 100 mL/ min) prior to and after reaction conditions, respectively.

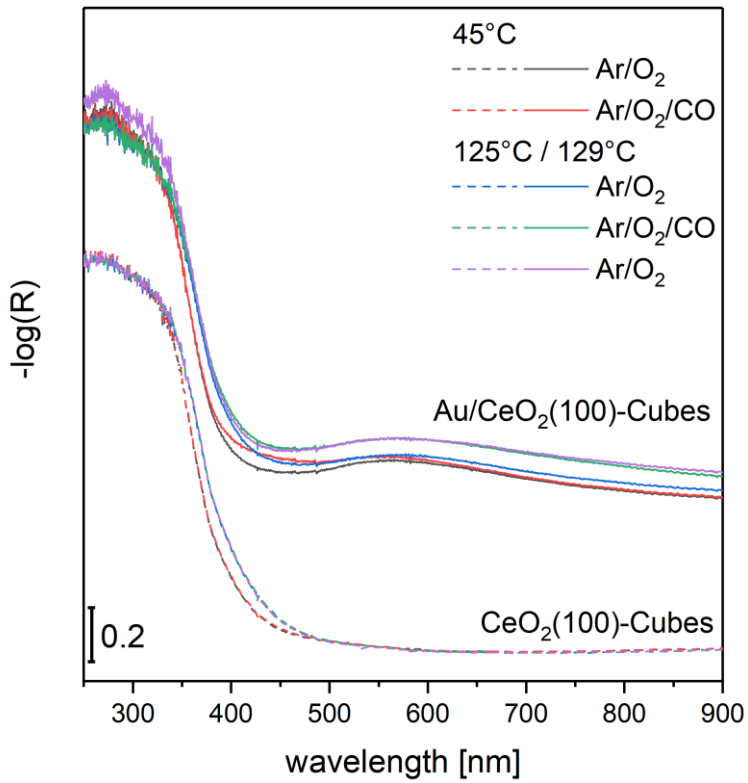


**Figure S6:** *Operando* UV-Vis spectra of the bare ceria cubes (at the bottom, dashed lines) and the gold-loaded cubes (at the top, solid lines). The spectra were recorded at the temperatures indicated, at a total flow rate of 100 mL/min, and feed compositions of 2% CO / 25% $O_2$ / Ar and 25% $O_2$ / Ar for reactive and oxidative conditions, respectively. Spectra of the gold-loaded samples were offset for clarity.

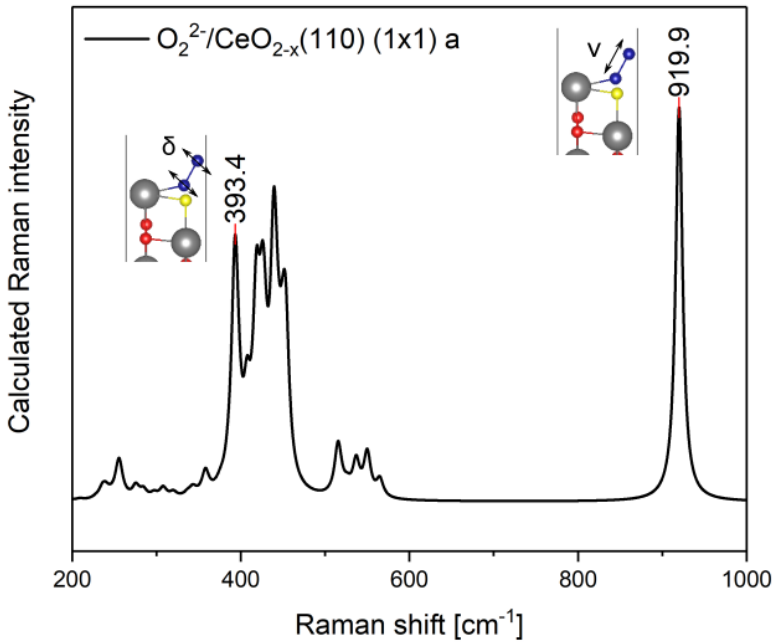


**Figure S7:** Calculated Raman spectrum for $O_2/CeO_{2-x}$(110) with (1×1) periodicity. The band positions of the peroxide vibrations are indicated together with the corresponding symmetry.

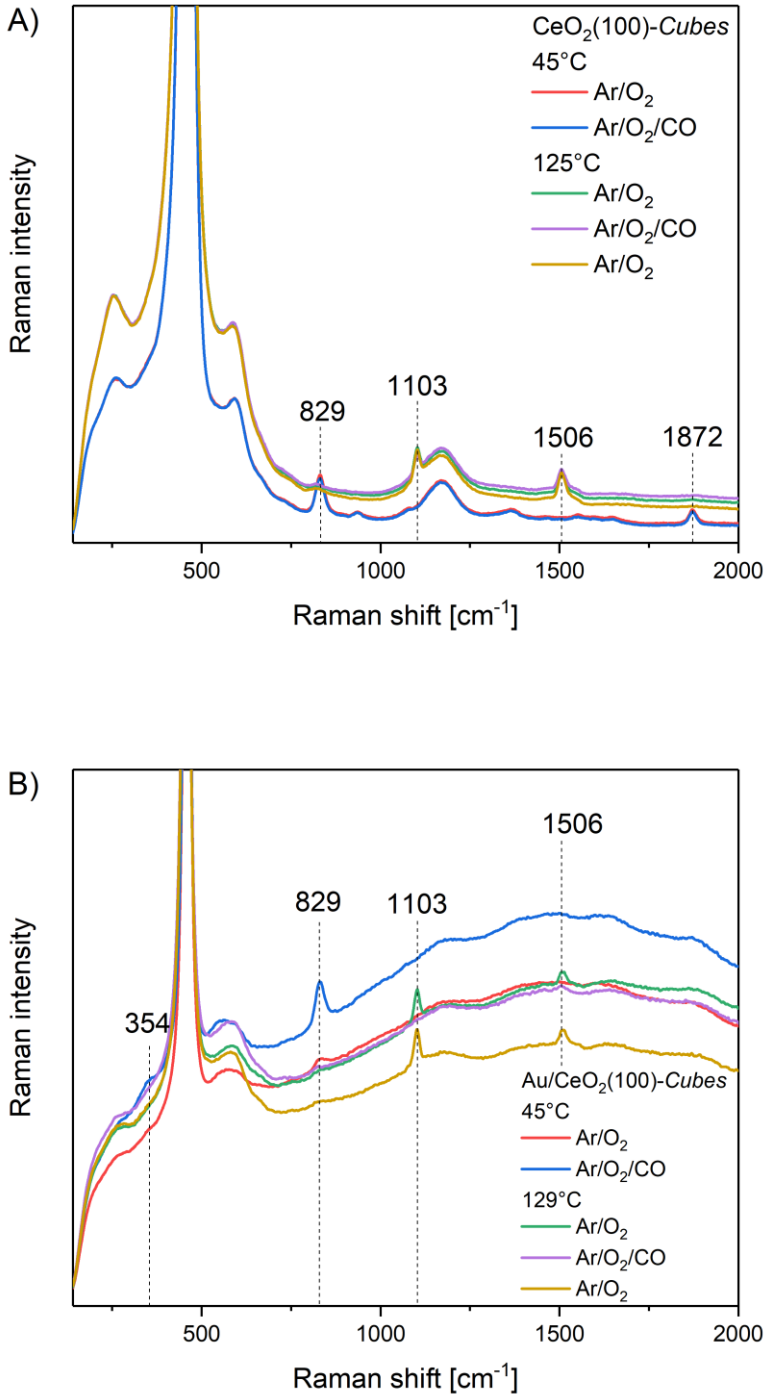


**Figure S8:** *Operando* 532 nm Raman spectra of **A)** bare ceria cubes and **B)** gold-loaded cubes. The spectra were recorded at the temperatures indicated, at a total flow rate of 100 mL/min, and feed compositions of 2% CO / 25% $O_2$ / Ar and 25% $O_2$ / Ar for reactive and oxidative conditions, respectively. The high intensity $F_{2g}$ peak at around 450 $cm^{-1}$ was cut off to allow an enlarged view of the other features. The band at 1103 $cm^{-1}$ is assigned to superoxides and the band at 1506 $cm^{-1}$ is assigned to weakly adsorbed oxygen on $CeO_2$(100).[1]

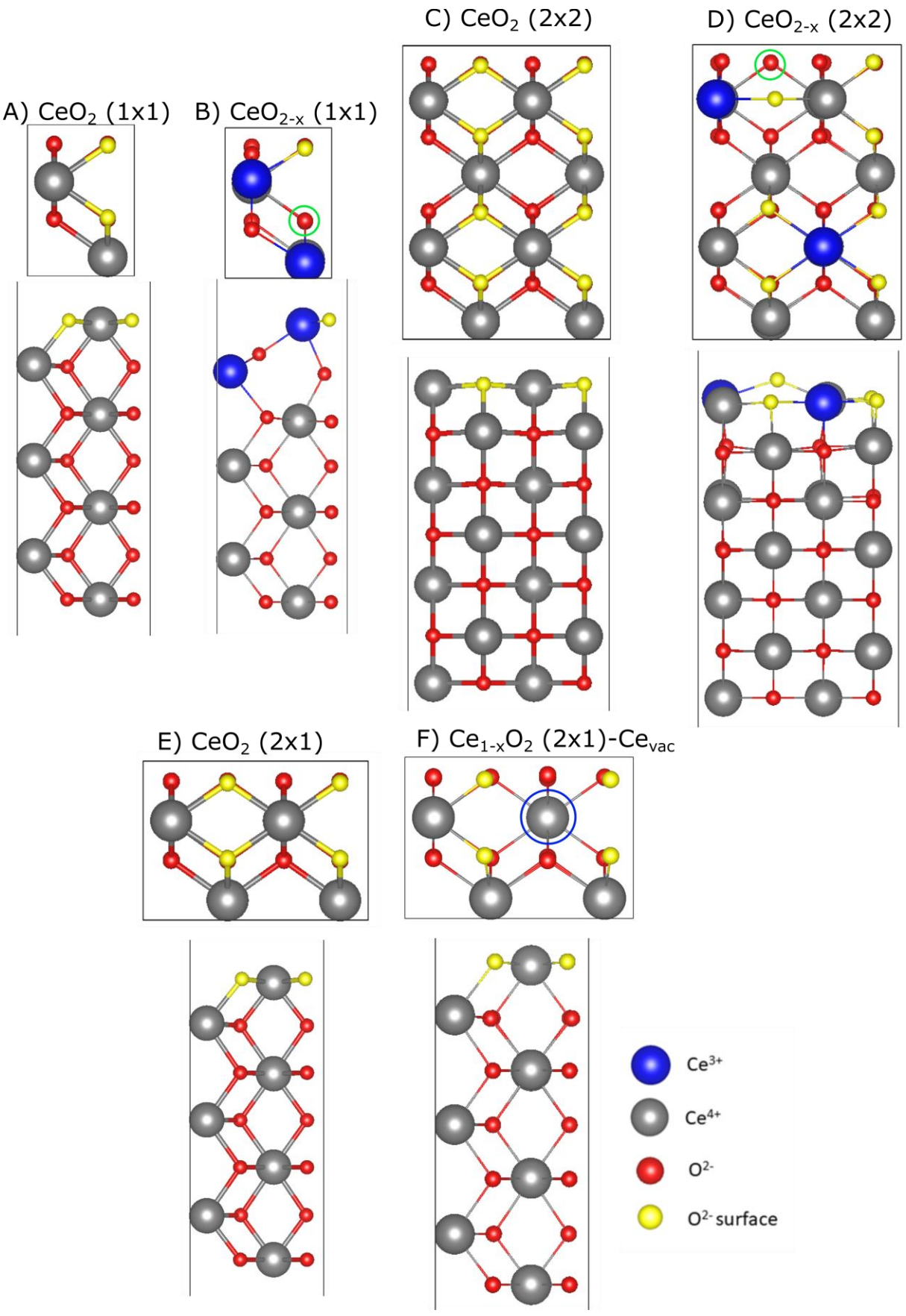


**Figure S9:** $CeO_2(110)$ unit cells with top and side view of the bare $CeO_2(110)$ and defective $CeO_{2-x}(110)$ as well as $Ce_{1-x}O_2(110)$ with (1×1), (2×1) and (2×2) periodicity, respectively. Atoms correspond to $Ce^{3+}$

(blue), $Ce^{4+}$ (grey), $O^{2-}$ (red), surface $O^{2-}$ (yellow) and the position of the oxygen/cerium vacancy is marked by a green or a blue circle, respectively.

**Table S1:** Total energies $E_{tot}$ for $CeO_2$(110) and for $CeO_{2-x}$(110) with (1×1)- and (2×2) periodicities. The defect formation energy $E_{vac}$ is given for the defective structures with respect to $E_{O_2}$ = -9.879 eV or $E_{Ce}$ = -1.489 eV, respectively.

*$E_{vac,\,O} = E_{CeO_{2-x}(110)} + 0.5\,E_{O_2} - E_{CeO_2(110)}$

**$E_{vac,\,Ce} = E_{Ce_{1-x}O_2(110)} + E_{Ce} - E_{CeO_2(110)}$

| **Structure** | **$E_{tot}$ / eV** | **$E_{vac}$ / eV** |
|---|---|---|
| A) $CeO_2$ (1×1) | -169.590 | - |
| B) $CeO_{2-x}$ (1×1) | -162.540 | 2.110* |
| C) $CeO_2$ (2×2) | -678.362 | - |
| D) $CeO_{2-x}$ (2×2) | -672.100 | 1.323* |
| E) $CeO_2$ (2×1) | -339.180 | - |
| F) $Ce_{1-x}O_2$ (2×1)- $Ce_{vac}$ | -319.991 | 17.700** |

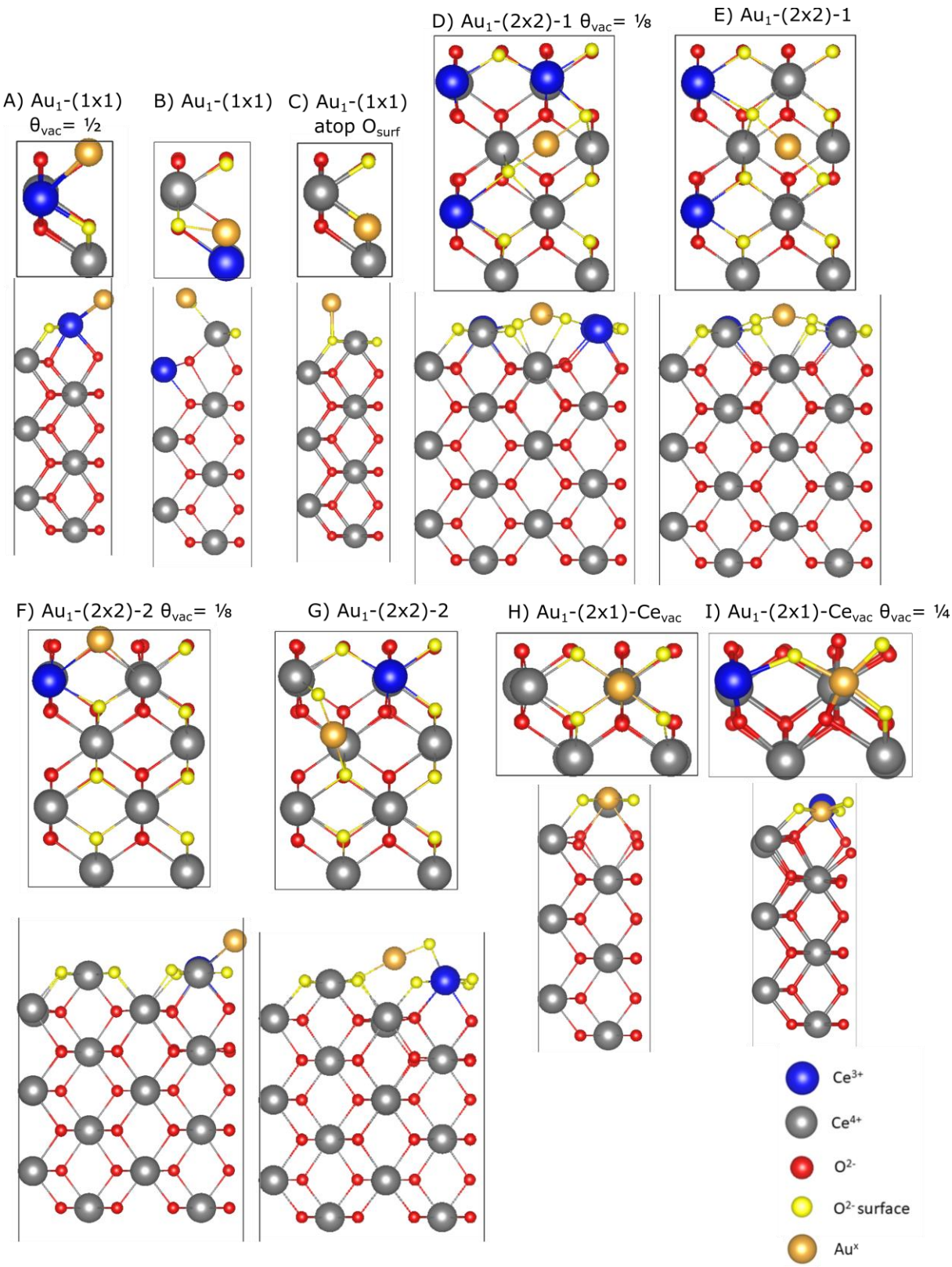


**Figure S10:** $CeO_2$(110) unit cells with top and side view of the most stable gold species on $CeO_2$(110) and $CeO_{2-x}$(110), respectively ((**A)** to **G)**). **H)** and **I)** show structures in which one cerium atom is substituted by a gold atom. The corresponding periodicities are indicated. Atoms correspond to $Ce^{3+}$ (blue), $Ce^{4+}$ (grey), $O^{2-}$ (red), surface $O^{2-}$ (yellow) and $Au^x$ (gold).

**Table S2:** Total energies $E_{tot}$ for gold deposited on $CeO_2(110)$ or $CeO_{2-x}(110)$ with (1×1)- and (2×2)-periodicities. The adsorption energy for gold $E_{ads,\,Au_1}$ is given with respect to $E_{Au_1}$ = -0.186 eV. Bader charges (ΔQ, in $|e|$) of the Au atoms are given in the last column.

| **Structure** | **$E_{tot}$ / eV** | **$E_{ads,\,Au_1}$ / eV** | **ΔQ** |
|---|---|---|---|
| A) $Au_1(1\times1)$ $\theta_{vac} = {}^1/_2$ | -164.858 | -2.131 | -0.64 |
| B) $Au_1(1\times1)$ | -171.645 | -1.869 | +0.44 |
| C) $Au_1(1\times1)$-atop $O_{surf}$ | -170.837 | -1.061 | -0.05 |
| D) $Au_1(2\times2)$-1 $\theta_{vac} = {}^1/_8$ | -673.630 | -1.340 | +0.25 |
| E) $Au_1$ (2×2)-1 | -679.817 | -1.269 | +0.62 |
| F) $Au_1(2\times2)$-2 $\theta_{vac} = {}^1/_8$ | -673,876 | -1.590 | -0.66 |
| G) $Au_1$ (2×2)-2 | -680,992 | -2.443 | +0.29 |
| H) $Au_1(2\times1)$-$Ce_{vac}$ | -326.350 | -6.549 | +1.18 |
| I) $Au_1(2\times1)$-$Ce_{vac}$ $\theta_{vac} = {}^1/_4$ | -321.603 | - | +1.09 |

Please note that for the structures in which one cerium atom is substituted by a gold atom the magnetic moments of the oxygen and cerium atoms were also analyzed, showing that the oxygen atoms in the immediate neighbourhood of the gold atom have magnetic moments, which is mostly indicative of $O^-$ states. This means that an one-electron transfer from gold to oxygen must take place. Futhermore, owing to the absence of $Ce^{3+}$ in structure H), a charge compensation can only take place through the presence of higher oxidation states than $Au^+$. These observations indicate a higher positive charge at the gold atom than the Bader charge analysis suggests, i.e., $Au^{3+}$ formation cannot be excluded and is highly probable, if gold adsorbs into a cerium vacancy.

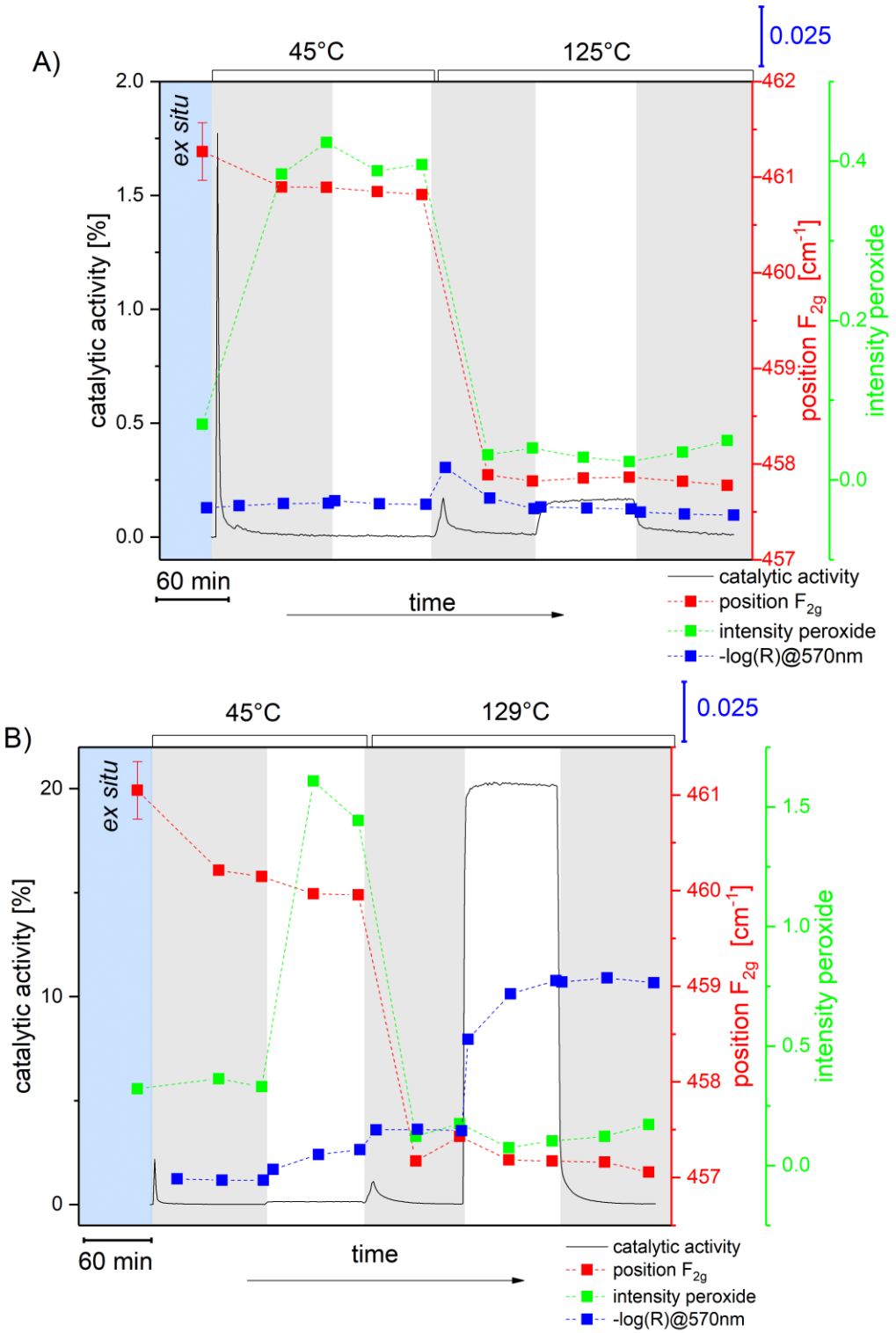


**Figure S11:** Summary of *operando* Raman and UV-Vis results for **A)** bare ceria cubes, and **B)** 0.6 wt% $Au/CeO_2$ cubes during CO oxidation (2% CO, 25% $O_2$, Ar) at a total flow rate of 100 mL/min at the temperatures indicated. Prior to and after reaction (grey area) the catalyst was treated in 25% $O_2$/Ar (white area). The measurement error for the $F_{2g}$ position is indicated exemplary for the *ex situ* measurement but applies to all $F_{2g}$ data points.

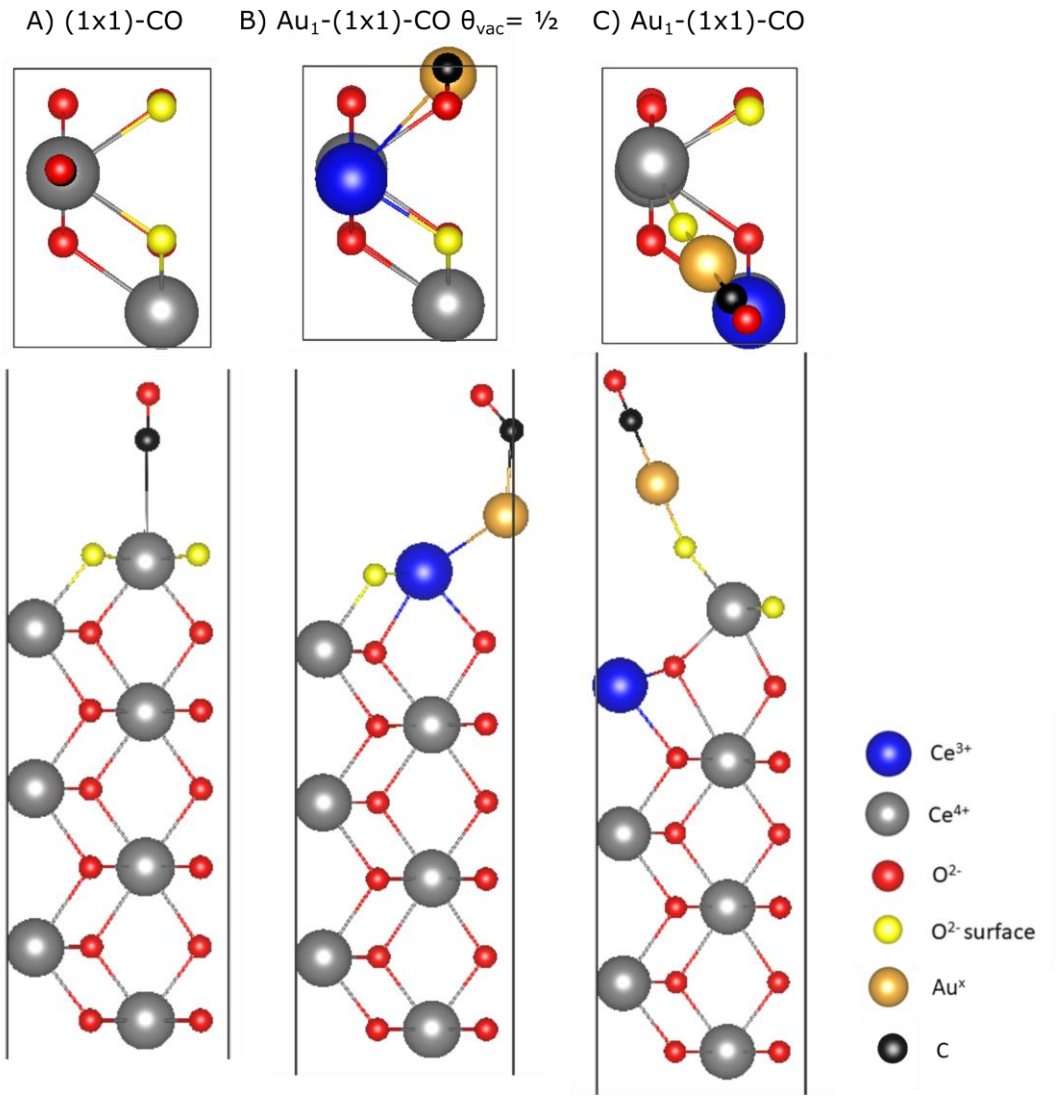


**Figure S12:** CO-$Au_1/CeO_2(110)$ and CO-$Au_1/CeO_{2-x}(110)$ unit cells with top and side view with (1×1) periodicity. Atoms correspond to $Ce^{3+}$ (blue), $Ce^{4+}$ (grey), $O^{2-}$ (red), surface $O^{2-}$ (yellow) $Au^x$ (gold) and C (black).

**Table S3:** Total energies $E_{tot}$ for CO adsorbed on $CeO_2(110)$, $Au_1/CeO_2(110)$ and $Au_1/CeO_{2-x}(110)$ with (1×1)- periodicities. The adsorption energy for CO $E_{ads,\,CO}$ is given with respect to $E_{CO}$ = -14.806 eV. Bader charges (ΔQ, in $|e|$) of the Au atoms are given in the last column.

| **Structure** | **$E_{tot}$** | **$E_{ads,\,CO}$*** | **ΔQ** |
|---|---|---|---|
| A) (1x1)-CO | -184.583 | -0.187 | - |
| B) $Au_1$(1×1)-CO $\theta_{vac} = 1/2$ | -179.899 | -0.235 | -0.48 |
| C) $Au_1$(1×1)-CO | -187.616 | -1.165 | +0.55 |

*$E_{ads,\,CO} = E_{CO@ceria} - (E_{CO} + E_{ceria})$

**References**


1 C. Schilling, M. V. Ganduglia-Pirovano and C. Hess, *J. Phys. Chem. Lett.*, 2018, **9**, 6593–6598.

2 C. Rajesh, S. Nigam and C. Majumder, *Phys. Chem. Chem. Phys.*, 2014, **16**, 26561–26569.